Novel low energy hydrogen–deuterium isotope breakthrough separation using a trapdoor zeolite
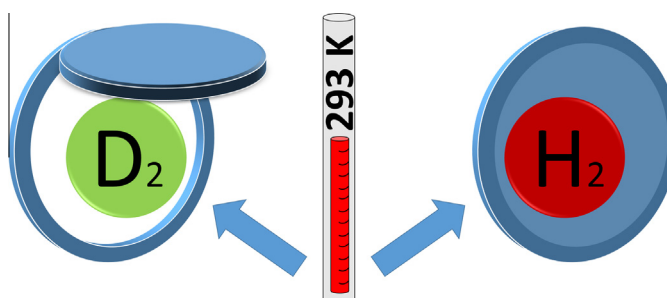
CrossMark

Andrew J.W. Physick [a], Dominic J. Wales [a], Simon H.R. Owens [a], Jin Shang [b], Paul A. Webley [b], Timothy J. Mays [a], Valeska P. Ting [a,*]

[a] Department of Chemical Engineering, University of Bath, Claverton Down, Bath, Somerset BA2 7AY, United Kingdom
[b] Department of Chemical and Biomolecular Engineering, University of Melbourne, Australia

HIGHLIGHTS

- Packed beds of "trapdoor zeolite" result in breakthrough separation of H_2 isotopes.
- Breakthrough separation of ^1H and ^2H occurs at ∼293 K.
- Interactions with trapdoor cations result in differences in breakthrough times.

GRAPHICAL ABSTRACT

ABSTRACT

Cs-chabazite, a type of zeolite with caesium counter-cations, possesses interesting gas separation properties due to a highly selective molecular "trapdoor" effect. Herein the use of this material for H_2/D_2 isotope separation is demonstrated. Isotope separation was achieved using breakthrough separation with a single pass through a packed bed at moderate temperatures (293 K) and pressures (0.17 MPa) when one species was in a sufficiently low concentration. The breakthrough separation curves were successfully modelled using the Thomas kinetic breakthrough model and the Yoon and Nelson kinetic breakthrough model, where working transferable kinetic rate constants were developed. Use of this material for hydrogen isotope separation would significantly lower the total energy demand compared with current hydrogen isotope separation techniques such as cryogenic distillation and is applicable to separating out low concentrations of D_2 (0.0156%) present in standard grade H_2.

1. Introduction

Over the last two decades, there has been a clear change in trend across the global community towards sustainable sourcing and more efficient use of fuels and chemical feedstocks, specifically concerning reductions in the use of finite fossil fuels. This has been most apparent at the governmental level, with policies such as the

UK Low Carbon Transition Plan [1] and international legally binding agreements such as the Kyoto Protocol 2020 [2], which focus on reducing CO_2 emissions. These are significant drivers for developing and implementing alternative, low carbon energy sources. In line with this global trend, there has been major financial and resource investment into large international collaborative projects (totalling over £17 billion) for unconventional energy generation, such as the Joint European Torus (JET) [3], Canadian Deuterium Uranium Reactors (CANDU) [4], the International Thermonuclear Experimental Reactor (ITER) [5] and the Tokamak Fusion Test Reactor (TFTR) [6]. These projects use large quantities of the hydrogen

isotope deuterium (^{2}H or D) as a feedstock fuel, which can cost up to €4000 per kg [7]. The demand for D_2 would increase dramatically if any of these three technologies were implemented on a wider scale in the future. Aside from such projects, ultrapure hydrogen (H_2) and deuterium (D_2) are already in high demand for application as deuterated chemical tracers, deuterated research grade chemicals and nuclear reactor heavy water moderators [8–10], driving the need for reductions in production costs for both chemical feedstocks, even at current production levels.

The most common method of producing ultrapure H_2 and D_2 is through separation of the isotopes from standard grade H_2 feedstock (standard grade H_2 composition: H > 99.98% and D < 0.0156% [11]), which is generated from steam reforming of natural gas by means of the water–gas shift reaction [12]. However, this fossil fuel-based method is ultimately unsustainable. Thus, alternative sources and methods for producing large-scale standard-grade H_2 and D_2 are being researched [13–15]. The liquid-based Girdler-Sulfide enrichment process can be used for initial D_2 enrichment of seawater up to ~20 wt%, but this is used exclusively for heavy water production for the nuclear power industry and its use is in sharp decline due to the large financial cost of operation and large quantities of poisonous H_2S produced [16]. The gas phase separation of hydrogen isotopes can be achieved either by cryogenic distillation at ~33 K [17,18], or through an absorption/chemisorption method using palladium (Pd) or vanadium (V) packed beds [19,20], both of which have extreme energy and financial cost penalties [21–22]. Other methods of hydrogen isotope separation have been investigated, but are uncommon due to the energy and financial costs [23–26].

There has been recent interest, by Hirscher et al. [27], in using nanoporous materials in a swing adsorption configuration (pressure, vacuum and temperature driven) for separating H_2 and D_2. The research has focused on the use of metal-organic frameworks (MOFs) [28,29] which have achieved highly pure separations, but only with low working pressures (0.001 MPa), low mass throughputs and small sample sizes due to the difficulty and expense of MOF synthesis and the degradation of MOFs with cycling. Another family of nanoporous materials that holds promise for isotope separations are zeolites, due to their low cost of production, widespread availability and mechanical and chemical stability [30]. However, little research has been done to date on the use of zeolites for hydrogen isotope separation [31,32]. The common, naturally-occurring chabazite branch of the zeolite family is of special interest for isotope separations due to an unusual selective trapdoor phenomenon reported by Webley et al. [33].

Caesium (Cs^+) chabazite (Cs-CHA) has a three-dimensional structure that consists of double six-ring prisms (6DR) arranged in layers linked by tilted four-membered rings (4MR) – see Fig. 1. Although large supercavities (6.7×10 Å) exist in the structure, eight-membered rings (8MR) that are 3.8 Å by 3.8 Å in diameter function as highly selective doorways, providing the only access to the crystal interior (Fig. 1). A Cs^+ cation is positioned energetically favourably in the centre of each of the 8MRs, balancing the charge of the framework and acting as selective aperture 'trapdoors' [34,35]. These trapdoors have a critical admission temperature (T_c) that is different for every gas (e.g. T_c for H_2 = 333 K) [36], above which the trapdoor is considered "open" and below which it is considered "closed". However, some gases, such as CO_2, have been reported to either not have a T_c, or for the T_c to be so low as for the trapdoor to be deemed permanently open, allowing for free gas access to the internal microporous supercavities.

A material allowing selective H/D separation without the need for cryogenic temperatures would vastly reduce the energy cost of hydrogen isotope separation, in comparison with the cryogenic distillation method currently used.
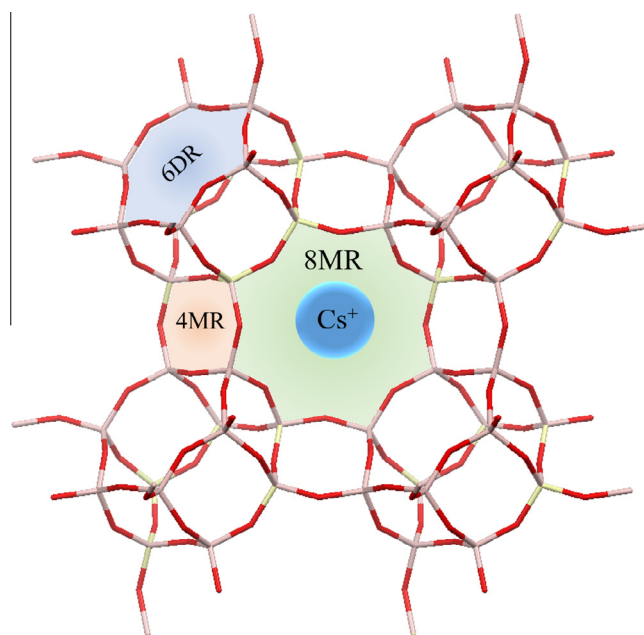

Fig. 1. Framework diagram of the Cs-chabazite structure, showing the 4MR (peach), 6DR (light blue) and 8MRs (light green) overlaid in bold, created using a crystallographic information file (cif) from Mazzi et al. [37] and Mercury (v3.5.1) software. Red = O, pink = Si, yellow = Al. (For interpretation of the references to colour in this figure legend, the reader is referred to the web version of this article.)

Studies into the selective trapdoor phenomenon of the chabazite structure [34,36,37] have thus far not investigated the effect that the H_2 and D_2 may have on the cation trapdoor. However, differences in the interactions of H_2 and D_2 with the cation trapdoor are predicted, based upon research into hydrogen isotope interactions with beryllium cations by Artiukhin et al. [38] and lithium cations by Czerwiński [39]. Based on this hypothesis, we aimed to test whether the selective trapdoor could be used to separate H_2 and D_2 at moderate temperatures (293–343 K) and pressures (0.17–1.00 MPa).

2. Materials and methods

Caesium (Cs^+) cation-exchanged chabazite zeolite material was synthesised in the Webley lab in accordance with previous reports [33]. Powder X-ray diffraction (PXRD) confirmed phase purity, thermogravimetric analysis (TGA) confirmed thermal stability up to 1173 K and N_2 sorption isotherms at 77 K showed low N_2 uptake, suggesting the pore-blockage for N_2 access due to the molecular trapdoor effect. Note that the presence of a small proportion of pores of 10 Å in width implies the existence of pore apertures not containing Cs^+ cations due to localised Al^{3+} deficiencies [40] (see Figs. S1–4 in Supplementary Information).

Breakthrough isotope separation experiments were conducted on a bespoke Hiden Isochema Isotope Exchange (IsoEx) rig. This rig consisted of a tubular reactor (0.6 Ø by 20 cm) held within a UniTemp BTZ-175E environmental chamber for precise reactor temperature control between 273 and 343 K, with an external reactor jacket heating coil for temperatures of 293–453 K (see Fig. 2). Hydrogen (H_2), deuterium (D_2) and argon (Ar) inlet pressures were controlled by three pressure transducers (GE Measurements and Control, PDCR 4020, 20 MPa) and gas flow was controlled by in-line mass flow controllers (Bronkhorst High Tech, M9208158C). A vacuum pump was used for in-line pre- and post-reactor degassing of the sample. A dynamic sampling mass spectrometer (Hiden Isochema, HPR-20 QCI) downstream of the reactor was used for exhaust gas detection.
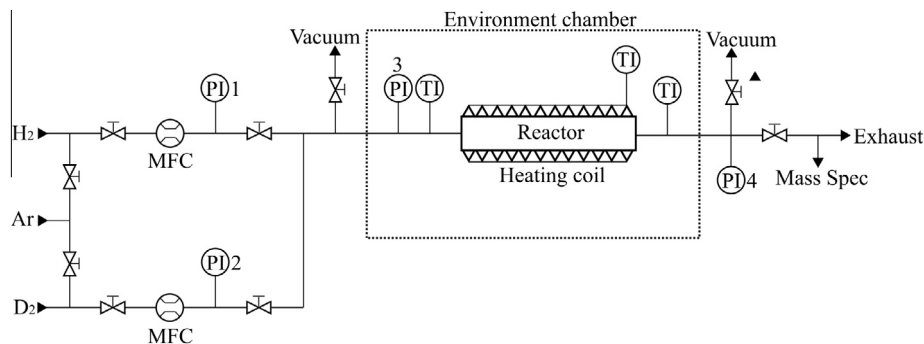
Fig. 2. Schematic of the IsoEx H$_2$–D$_2$ separation rig. PIs are pressure indicators, TIs are temperature indicators and MFCs are mass flow controllers.

Three packed beds of caesium chabazite from a single synthesis batch were used for the breakthrough measurements. The white Cs$^+$ chabazite solid was ground gently in an agate mortar and pestle to a fine powder before being degassed in a Micromeritics ASAP 2020 (heated to 623 K at 5 K min^{-1}, evacuated at 0.003 MPa min^{-1} to 9×10^{-5} MPa for 36 h, then held under vacuum whilst cooling). The prepared samples (Table 1) were then promptly transferred into the IsoEx reactor and packed into a reactor volume of 1.98 cm^3 for sample 1 (0.6 Ø $\times$ 7 cm) and 1.13 cm^3 for samples 2 and 3 (0.6 Ø $\times$ 4 cm). The samples were degassed *in-situ* for 1080 min at 453 K prior to each breakthrough experiment.

3. Results

3.1. Pressure effects on hydrogen breakthrough in Cs$^+$ chabazite

To determine the effect of pressure changes on the breakthrough times of gas through the Cs$^+$ chabazite packed bed, three pressures (measured using PI1–3, Fig. 2) of ultra-pure H$_2$ (0.17, 0.40 and 1.00 MPa) were tested at 293 K (Fig. 3) on sample 1 and the start of the H$_2$ breakthrough times (B_S) and complete breakthrough times (B_F), at each pressure, were compared (H$_2$ sourced from Air Products, BIP-Plus, 99.99996%). The raw breakthrough data y-axis had units of Torr generated from the mass spectrometer ion counts from a throttled sampling capillary on the reactor exhaust. Due to the throttled capillary and the automatic spectral deconvolution (ASD) algorithm in the MassSoft Professional software (v6.21.0.51), the Torr counts could not be correlated to a specific mass throughput. However, scaling in terms of concentration (C) over final concentration (C_0) was possible (Figs. 3–11).

The B_S time for the 0.17 MPa run was 8.5 min and the B_F was 40 min, which was approximately double the B_S and B_F times ($\sim$175% and 220%) for the 1.00 MPa and triple the B_S and B_F times ($\sim$340% and $\sim$330%) of the 0.40 MPa run—a considerably longer breakthrough time. Interestingly the B_S and B_F times for the 1.00 MPa were lower than for the 0.40 MPa. This shows that the

Table 1
The specific chabazite packed bed dimensions of the three samples and the associated experiments. Chabazite sample density, ρ_p, is 2.245 g cm^{-3} (see Supplementary Information Section 1.2).

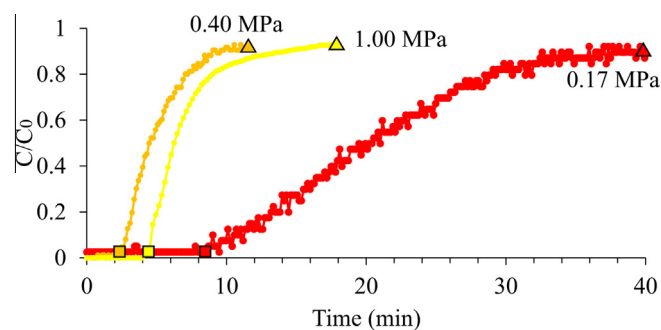| Sample	Bed length (cm)	Sample mass dry (g)	Bulk density (g cm^{-3})	Voidage	Experiments
1	7	3.51	1.77	0.21	Pressure effect
2	4	1.98	1.13	0.22	Temperature effect
3	4	1.98	1.13	0.22	Isotope separation

Fig. 3. A comparison of the pure hydrogen breakthrough in Cs$^+$ chabazite at 0.17, 0.40 and 1.00 MPa, with the molecular trapdoors in the closed state (293 K). In comparison to the 0.17 MPa, both the B_S (squares) and B_F (triangles) decrease with an increase in pressure.
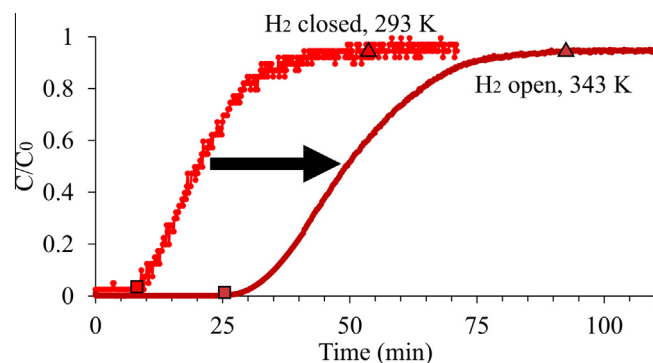

Fig. 4. Pure H$_2$ breakthrough curves in Cs$^+$ chabazite with the molecular trapdoor in both the closed (293 K) and open (343 K) states. The B_S (squares) and B_F (triangles) increased by 315% and 220% when the trapdoors were opened, indicating a strong H$_2$ dependence on the trapdoor position. H$_2$ passes through the interstitial space when trapdoors are closed and the porous interior when open.

lower pressure gas actually starts to breakthrough before the higher pressure, and also fully breaks through before the higher pressure. As the value of B_S is the only difference between the 0.40 and 1.00 MPa runs, this suggests that the packed bed was distorted by a fluid hammer effect at higher pressures, reducing the packed bed interstitial space due to compression. For breakthrough separation systems, a large mass transfer region (S breakthrough curve region in Figs. 3–11) with respect to time is desirable, to ensure that as much of the separation material is utilised as possible and thus minimising the time between column regenerations. This also increases the breakthrough time difference between the species to be separated, highlighting the preference for longer
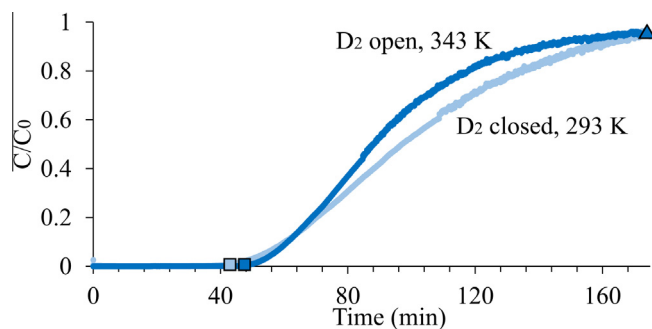
Fig. 5. Pure D_2 breakthrough curves in Cs^+ chabazite with the molecular trapdoor in both the closed (293 K) and open (343 K) states. Unlike the H_2, the B_S (squares) and B_F (triangles) for D_2 were unaffected by the trapdoor position (open/closed).

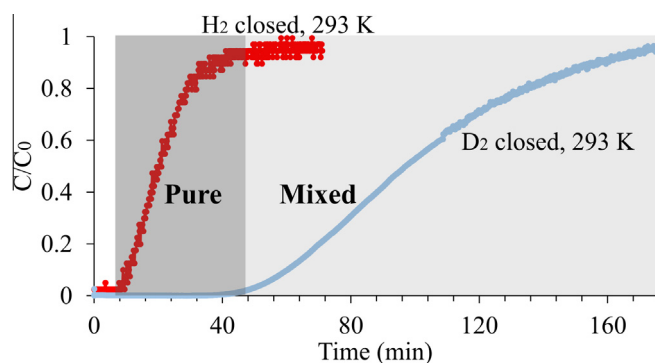**Fig. 6.** H_2 and D_2 breakthrough curves in the Cs^+ chabazite with the molecular trapdoors in the closed state at $T = 293$ K. There is a significant difference (>50 min) between the values of B_S and B_F for the H_2 and D_2, which showed that a pure separation with a single pass is possible. The darker region represents the time period over which a single, pure isotope species is flowing out of the packed bed, meaning a separation of the two isotopes is possible.

Fig. 7. Comparison of the H_2 and D_2 breakthrough curves in the Cs^+ chabazite with the molecular trapdoors in the open state ($T = 343$ K). There is still a separation between the B_S and B_F for the H_2 and D_2 but to a lesser extent, despite the H_2 now having access to the porous interior. The darker region represents the period over which a single, pure isotope species is flowing out of the packed bed, meaning a separation of the two isotopes is possible, but not ideal.
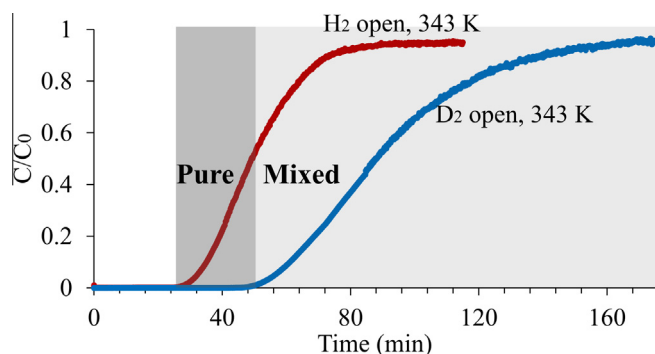

Fig. 8. Comparison of the four separate H_2 and D_2 breakthrough curves in the Cs^+ chabazite with the molecular trapdoors in both the open and closed states, numbered in order of breakthrough measurements. The B_S (squares) and B_F (triangles) are shown for each breakthrough.

Fig. 9. Breakthrough of a 50 wt% mix of H_2 and D_2 in Cs^+ chabazite at 1.7 bar on sample 3, with the molecular trapdoors in the closed state at 293 K.
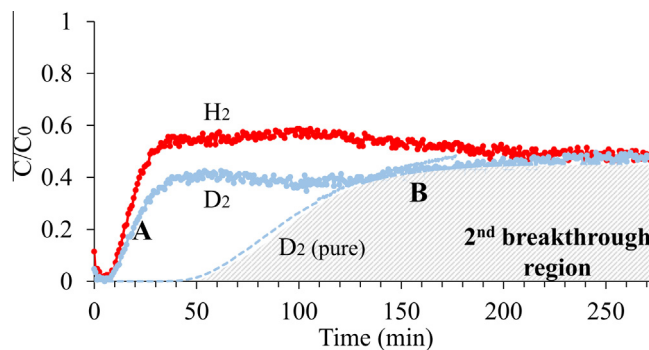
Fig. 10. Breakthrough of a 50 wt% mix of H_2 and D_2 in Cs^+ chabazite at 1.7 bar, with the molecular trapdoors in the closed state at 293 K, with an extended breakthrough time. The pure D_2 breakthrough (from Fig. 5) is overlaid, which matches the secondary breakthrough region.

breakthrough times. Furthermore, for this specific breakthrough system, with shorter breakthrough times, fewer counts are available for the mass spectrometer whilst in Multiple Ion Detection (MID) mode. Therefore, a pressure of 0.17 MPa was chosen for the H_2–D_2 breakthrough experiments.

A working pressure of 0.17 MPa could be considered low and unsuitable for use within industry due to the low gas density of H_2 and D_2, and thus low mass throughputs. Nevertheless, if the
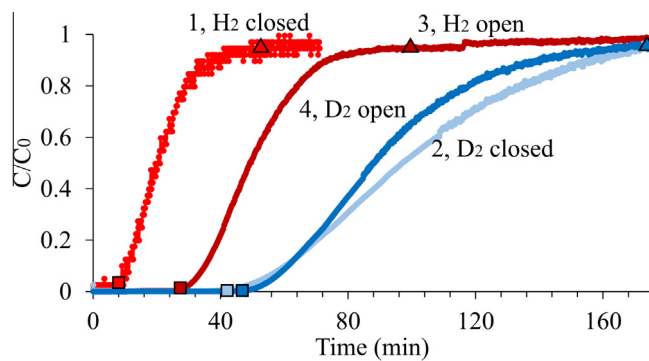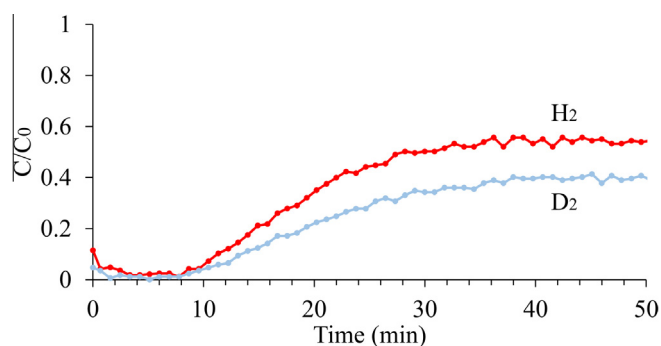
system were to be scaled up, and the packed bed length and reactor cross sectional area increased, the ideal working pressure could also be increased accordingly. Note that the static working pressures tested in MOF based H_2–D_2 separation systems have been considerably lower then the 0.17 MPa tested in this work [27–29], justifying the selection of working pressure in this study.

3.2. Temperature effects on hydrogen and deuterium breakthrough in Cs^+ chabazite

Four separate breakthrough measurements on Cs^+ chabazite were made on sample 2 using ultrapure D_2 (D_2 sourced from Air Products BIP-Plus, 99.99996%) or ultra-pure H_2 with the trapdoor

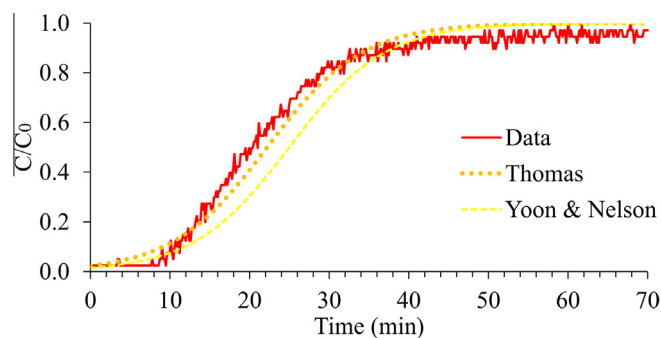**Fig. 11.** An example of the Thomas model and the Yoon and Nelson model applied to the pure H_2 breakthrough with the trapdoors in the open state ($T = 343$ K). The Thomas model has a chi squared (χ^2) of 19.8, whereas the Yoon and Nelson model has a χ^2 of 48.3 with 1 degree of freedom. Visually the Thomas model appears to be the best fit, but the Yoon and Nelson model is statistically the best fit in this case according to the χ^2 method.

gates either in the open and closed positions ($T = 343$ and 293 K). Phase purity of the Cs^+ chabazite was unaffected by repeat cycling (>20 heating cycles) in the IsoEx, as confirmed by PXRD before and after loading into the reactor (see Fig. S4 Supplementary Information).

The breakthrough of H_2 was found to be highly dependent on the trapdoor state (Fig. 4), with the B_S and the B_F increasing by 315% and 220% from the trapdoor closed to open positions. This suggests that H_2 can only pass though the interstitial space when the molecular trapdoors are closed. When the trapdoors are open the H_2 can also pass through the microporous supercavity interior, decreasing the mean free path (MFP) of the H_2 molecules and thus, increasing total travel time through the bed. This can be explained by $dP = e^{-x/\mu} dx$, where dP is the probability that a collision will not happen between two points of travel (x and $x + dx$), and the constant μ is the mean free path (MFP, mean time travelled between two collisions). The increase in total travel time is caused by a decrease in the value of MFP (μ) which in turn decreases the value of dP, and thus, increases the probability of a collision over a fixed distance through the packed bed. This can be further explained by the cubic lattice random walk model, where an increase in the number of collisions (or distinct sites, $S(t)$) directly increases the total travel time [41].

Interestingly D_2 breakthrough kinetics were found to be completely independent of the trapdoor state (Fig. 5), with the B_S and B_F remaining unchanged, implying that the T_C for D_2 is out of the experimental operating range (293–343 K).

The independence of the D_2 and the dependence of the H_2 in relation to the trapdoor state is shown in Fig. 6, where the B_S and B_F of D_2 are approximately 5 times and 4 times of the values of H_2 when the trapdoor is closed (at $T = 293$ K). The longer total time for D_2 shows that the trapdoor state independence of D_2 is not one of exclusion, but rather one of irrelevance, as D_2 can pass through the closed trapdoor. This suggests that the T_C for D_2 is lower than the experimental temperature range investigated here. H_2–D_2 breakthrough crossover is a main limiting factor for Pd and V based separation systems [42], but in Fig. 6 no breakthrough crossover is present (onset time of D_2, B_S > end time of H_2, B_F). This is due to the decrease in MFP for the D_2 (and thus increase in total path time) passing through the closed trapdoors and the MFP remaining unchanged for the H_2 (no increase in the total path time) due to H_2 not passing through the closed cation trapdoors. This allows for simple, highly pure hydrogen isotope separations at room temperature (293 K) and moderate pressures (0.17 MPa) using an inexpensive and easily synthesised Cs^+ chabazite material, potentially lowering the energy requirement for such separations significantly compared with well established cryogenic distillation systems (~33 K [17,18]) and MOF based systems (~77 K [27]).

It would be expected that the start of the H_2 and D_2 breakthroughs would match when the trapdoor position is open, such that H_2 B_S = D_2 B_S, as H_2 gas could then access the interior microporous supercavities, similar to the D_2, but this is not the case as seen in Fig. 7. One explanation is that the H_2 cannot access the same interior channels as the D_2. Kohen et al. [43] recently reported atomic simulations on chabazite trapdoor positions which suggest the cation trapdoors rapidly and temporarily displace into the internal supercavities and 4MRs giving rise to the 'open' state position [44–47]. If the frequency of cation movement within the internal pores is high, new temporary internal trapdoors may be formed, blocking access to some of the internal channels for H_2, but again not affecting D_2 due to its trapdoor independent behaviour at the experimental temperature range investigated here. This would account for H_2 B_S < D_2 B_S seen in Fig. 6. For pure, or high concentration systems, separation of the isotopes would be viable in a single cycle, compared to a minimum of 8 cycles for the same result in MOF based systems [27]. The H_2 and D_2 breakthroughs whilst in the open and closed state can be seen in Fig. 8.

3.3. H_2:D_2 50:50 weight% breakthrough experiments

To test whether the material is suitable for enrichment-type separations where the concentration of one isotope may approach the concentration of the other (similar to the Girdler-Sulfide enrichment process), breakthrough measurements were conducted using a 50 wt% gas mixture of H_2 and D_2 (sourced from BOC, 50 wt% D_2, balance H_2, 99.99996%) at 293 K on sample 3.

The H_2 in the binary gas mixture (Fig. 9) had similar breakthrough properties as reported in Fig. 3), with the exception that the final concentration ratio was lower and did not reach $C/C_0 = 1$ (0.6 compared with 1.0 C/C_0). This was in part due to the concentration of each individual species being reported in terms of the initial concentration of the pre-mixed binary inlet gas. The D_2, however, did not match the high D_2 concentration breakthrough times seen in Fig. 5, and was comparable to the H_2 breakthrough regime instead. Interestingly, the final concentration ratio of the H_2 was ~0.6, and only ~0.4 C/C_0 for the D_2, after 50 min. The inlet concentration ratio was 0.5 C/C_0 for both H_2 and D_2, suggesting that there was either an accumulation of D_2 within the chabazite, or that there was a percentage of D_2 passing through an auxiliary pathway much more slowly (>50 min) than the remainder of the bulk gas through the packed bed.

When the experimental breakthrough time was extended to 275 min (Fig. 10), there was a noticeable change in the concentration ratio at ~125 min, with what seemed to be a secondary D_2 breakthrough curve. When compared to the high D_2 concentration breakthrough times (Fig. 5), the apparent secondary breakthrough curve at ~125 min for the binary system matched the high D_2 concentration breakthrough curve, as shown in Fig. 10. The C/C_0 of the data shown in Fig. 5 above was scaled to 0.5, so that comparison with D_2 in the 50% binary system was possible in Fig. 10. This confirms that there is no accumulation of D_2 within the chabazite, but rather that there are two accessible pathways for the D_2 to pass through the packed bed when H_2 is present in moderate concentrations (50 wt%). The first pathway is proposed to be through the interstitial space along with the H_2, which is notably not seen when an extremely low concentration of H_2 is present in a dominant, almost pure D_2 flow (Fig. 5), shown by the first D_2 breakthrough (A in Fig. 10). This is believed to be caused by the H_2 partially blocking access to the trapdoor openings (8MR) on the outside of the porous framework for part of the D_2 flow, as the H_2 was passing through the interstitial space, and thus over the 8MRs. The second pathway is through the Cs^+ chabazite trapdoors and into the porous interior, increasing the MFP and thus, the breakthrough time, which is seen for very low concentrations

Table 2

Modelled kinetic rate constants for the breakthrough runs of H_2 with the trapdoors open and closed, D_2 with the trapdoors open and closed (T = 343 K and 293 K) and the 50 wt% H_2–D_2 mix. The units are K_{Th} (ml min^{-1} mg^{-1}), q_{Th} (mg g^{-1}), K_{YN} (l min^{-1}), torr (t @ 50% breakthrough, min).

	Thomas				Yoon and Nelson			
	K_{Th}	q_{Th}	χ^2	p-Value	K_{YN} ($\times 10^{-1}$)	τ ($\times 10$)	χ^2	p-Value
H_2 closed	3.75×10^{-5}	1.66×10^6	4.600	0.0319	1.67	2.50	7.254	0.0070
H_2 open	3.14×10^{-5}	3.25×10^6	19.815	0.0000	1.13	4.95	48.317	0.0000
D_2 closed	1.19×10^{-5}	9.55×10^6	24.225	8.5735×10^{-7}	0.61	9.71	44.322	0.0000
D_2 open	1.26×10^{-5}	6.59	276.049	0.0000	0.45	8.78	1522.087	0.0000
H_2 50 wt%	10.75×10^{-5}	1.14×10^3	10.510	0.0011	2.60	1.76	2.797	0.0944
D_2 50 wt%	1.30×10^{-4}	9.11×10^2	1.099	0.2944	1.70	2.47	1.449	0.2208

of H_2 in a dominant D_2 flow, shown by the second D_2 breakthrough (B in Fig. 10).

This indicates that Cs^+ chabazite could be used to separate out low concentrations of isotopes from a standard grade hydrogen gas feedstock, where the concentrations are extremely low ($\sim$0.0156%). Cs^+ chabazite could also possibly be a suitable material for the initial enrichment of D_2 in a multi pass breakthrough system, but enrichment would become severely limited above 50 wt%.

3.4. Kinetic breakthrough modelling

Kinetic rate breakthrough modelling was applied to the breakthrough measurements, in order to develop a robust kinetic rate equation that is applicable to Cs^+ chabazite hydrogen isotope separation systems, to aid in the design of future systems. Two models were investigated in parallel for robustness of design: the Thomas kinetic breakthrough model, also known as the bed depth service time (BDST) model, and the Yoon and Nelson kinetic breakthrough model [48]. Both models are regularly used to model gas breakthrough and separations through packed beds. The Pearson's chi-squared (χ^2) method of goodness of fit was applied to the polynomial S-type breakthrough curve fittings, and the coefficient of determination (R^2) method of goodness of fit was applied to the linear forms of the kinetic models.

The first model applied was the Thomas kinetic breakthrough model, which is a simplified form of the Bohart and Adams [49] irreversible isotherm model. In simplifying the model, the interparticle mass transfer resistance and the external resistance are excluded, meaning the surface interaction between the adsorbate and unspent adsorbent controls the rate of adsorption, and thus, the breakthrough. The Thomas model has two Thomas rate constants: the kinetic rate constant of K_{Th} (ml min^{-1} mg^{-1}) and the maximum solid phase concentration of the solute constant of q_{Th} (mg g^{-1}). The Thomas model is reliant upon the known specific system parameters of volumetric gas flow rate Q (ml min^{-1}), gas throughput volume V (ml), mass of the adsorbent M (g), the inlet concentration C_0 (mg l^{-1}) and the rate constants. To apply the model, the real $\ln\left(\left(\frac{C_0}{C}\right) - 1\right)$ vs. V was plotted, which had a gradient of $-K_{Th}C_0/Q$ and an intercept of $K_{Th}q_{Th}M/Q$ which were used with the linearised form to calculate the Thomas rate constants K_{Th} and q_{Th}. The constants could then be used in Eq. (1) to model the breakthrough curves, as seen in Fig. 11. The Thomas model is known to suffer deficiencies at $t = 0$ because of the C_0 component on the right hand side of the model, severely overestimating the C/C_0 at this time point.

Thomas model:

$$\frac{C}{C_0} = \frac{1}{1 + \exp\left[\frac{K_{Th}}{Q}(q_{Th}M - C_0V)\right]} \tag{1}$$

Linearised form of the Thomas model:

$$\ln\left(\frac{C_0}{C} - 1\right) = \frac{K_{Th}q_{Th}M}{Q} - \frac{K_{Th}C_0}{Q}V \tag{2}$$

The second model used was the Yoon and Nelson kinetic breakthrough model [50–51], which is based upon the assumption that the rate of decrease in the probability of adsorption for each adsorbate molecule is directly proportional to the probability of adsorbate breakthrough on the adsorbent. The Yoon and Nelson model also has two rate constants: the kinetic rate constant of K_{YN} (l min^{-1}) and the 50% adsorbate breakthrough time constant of τ (min). The Yoon and Nelson model is only reliant upon the specific system time (t) and the rate constants, making the model easier to apply if a number of the specific system variables are unknown. The model was applied by plotting the real $\ln\left(\left(\frac{C_0}{C}\right) - C\right)$ vs. t, which had a gradient of K_{YN} and an intercept of $-\tau K_{YN}$ which were used in the linearised form of the model to calculate the rate constant. The constant could then be used in Eq. (3) to model the breakthrough curves, as seen in Fig. 11. The Yoon and Nelson model does not suffer from the same $t = 0$ issue as the Thomas model as there is no C_0 component on the right hand side.

Yoon and Nelson model:

$$\frac{C}{C_0} = \frac{1}{1 + \exp[K_{YN}(\tau - t)]} \tag{3}$$

Linearised form of the Yoon and Nelson model:

$$\ln\left(\frac{C}{C_0 - C}\right) = K_{YN}t - \tau K_{YN} \tag{4}$$

To determine the goodness of fit, the chi-squared (χ^2) method was used (see Supplementary Information for details). There was a large increase in the χ^2 value for the H_2 and D_2 when the trapdoors were changed from the closed to the open states, leading to a decrease in the p-value for each. Statistically the Yoon and Nelson model outperformed the Thomas model for all of the pure species breakthroughs and also the D_2 component of the 50 wt% gas mixture breakthrough (confirmed by lower p-values from the χ^2 statistical test, Table 2). The Thomas model statistically only outperformed the Yoon and Nelson model for the H_2 component of the 50 wt% gas mixture breakthrough. Therefore for maximum separation of low concentrations of D_2 from a high H_2 concentration, the Yoon and Nelson kinetic parameters of $K_{YN} = 1.67 \times 10^{-1}$ l min^{-1} and $\tau = 25$ min should be used.

4. Conclusion

A low-energy breakthrough separation technique was investigated for use in separating two isotopes of hydrogen. D_2 breakthrough was only partially independent of the trapdoor position or occupancy when D_2 was present in concentrations of 50 wt%. A two-stage D_2 breakthrough was observed, possibly due to a proportion of the D_2 passing through the interstitial space along with the H_2, and the remainder passing through the closed trapdoors, leading to an increase in the MFP and breakthrough time. H_2 was completely excluded, even when the trapdoors were in the open position when H_2 was in the lower concentration of 50 wt%, causing the H_2 to pass through the interstitial space. This suggests that

the affinity of the chabazite packed bed towards D_2 is much greater than for H_2, even when the trapdoor gates are in the open position, confirming the predicted difference in the interaction of H_2 and D_2 with the cation trapdoor. The elucidation of the role of the Cs^+ cation in discriminating between different gas species for separations will be the subject of further study.

This work demonstrates that Cs^+ chabazite packed bed breakthrough separation is not suitable when the concentration of either species increases beyond low percentile amounts, so would not be appropriate for multi-pass enrichment configurations. However, for industrial applications, this is not an issue, as most H_2–D_2 separation systems are either based upon separating trace amounts of D_2 from a H_2 feedstock sourced from the water–gas shift reaction of natural gas, or upon separating trace amounts of H_2 from a D_2 feedstock to create ultra-pure D_2.

D_2 breakthrough was found to be independent of the trapdoor position or occupancy when D_2 was present in high concentrations, so appears to have a threshold admission temperature T_C at a temperature lower than the experimental range investigated. H_2 is highly dependent on trapdoor position when in high concentrations, only passing through the trapdoors when in the open position. Due to the differences in the interactions, no breakthrough crossover was observed for the high concentration breakthrough measurements when the trapdoors were in the closed position. Therefore, Cs^+ chabazite packed bed breakthrough separation is possible at moderate temperatures (293 K) and pressures (0.17 MPa) when one species is in a sufficiently low concentration, significantly lowering the total energy demand compared to current cryogenic distillation methods [16,17,20,21]. This could be a new method for separating D_2 from standard grade H_2 due to the low concentrations of D_2 present (0.0156%).

Acknowledgments

Appendix A. Supplementary data

Supplementary data associated with this article can be found, in the online version, at http://dx.doi.org/10.1016/j.cej.2015.11.040.

References

[1] Department of Energy and Climate Change, The UK Low Carbon Transition Plan, 2009. Available at: <https://www.gov.uk/government/publications/the-uk-low-carbon-transition-plan-national-strategy-for-climate-and-energy> (accessed November 2015).

[2] UNFCCC, Kyoto Protocol to the United Nations Framework Convention on Climate Change. Kyoto: UN (30822), 1998.

[3] E. Bertolini, D. Eckhartt, A. Gibson, J.P. Poffé, P.H. Rebut, D.L. Smart, The JET Project: Design Proposal for the Joint European Torus, second ed., Commission of the European Communities Directorate General Scientific and Technical Information and Information Management, Luxembourg, 1976.

[4] L.G. Brookes, H. Motamen (Eds.), The Economies of Nuclear Energy, second ed., Chapman & Hall, U.K., 1984.

[5] T.W. Overton, Fabrication begins for ITER fusion reactor central solenoid, Power 159 (2015) 8.

[6] F.M. Levinton, M.C. Zarnstorff, S.H. Batha, M. Bell, R.E. Bell, R.V. Budny, C. Bush, Z. Chang, E. Fredrickson, A. Janos, J. Manickam, A. Ramsey, S.A. Sabbagh, G.L. Schmidt, E.J. Synakowski, G. Taylor, Improved confinement with reversed magnetic shear in TFTR, Phys. Rev. Lett. 75 (1995) 4417–4420.

[7] R. Arnoux, Deuterium: a precious gift from the Big Bang, ITER Newsline 167 (2011) 3.

[8] J. Thierrin, G.B. Davis, C. Barber, A groundwater tracer test with deuterated compounds for monitoring in-situ biodegradation and retardation of aromatic-hydrocarbons, Ground Water 33 (1995) 469–475.

[9] G.R. Fulmer, A.J.M. Miller, N.H. Sherden, H.E. Gottlieb, A. Nudelman, B.M. Stoltz, J.E. Bercaw, K.I. Goldberg, NMR chemical shifts of trace impurities: common laboratory solvents, organics, and gases in deuterated solvents relevant to the organometallic chemist, Organometallics 29 (2010) 2176–2179.

[10] H. Mochizuki, M.H. Koike, T. Sakia, Core coolability of an ATR by heavy-water moderator in situations beyond design basis accidents, Nucl. Eng. Des. 144 (1993) 293–303.

[11] F. Pavese, On problems in the definition of the International Temperature Scale arising from the variability of the isotopic composition of some substances used for the fixed-points, Metrologia 42 (2005) 194–200.

[12] J.G. Xu, G.F. Froment, Methane steam reforming, methanation and water–gas shift. 1. Intrinsic kinetics, AIChE J. 35 (1989) 88–96.

[13] K. Christopher, R. Dimitrios, A review on exergy comparison of hydrogen production methods from renewable energy sources, Energy Environ. Sci. 5 (2012) 6640–6651.

[14] D.B. Levin, R. Chahine, Challenges for renewable hydrogen production from biomass, Int. J. Hydrogen Energy 35 (2010) 4962–4969.

[15] A.O. Menezes, M.T. Rodrigues, A. Zimmaro, L.E.P. Borges, M.A. Frage, Production of renewable hydrogen from aqueous-phase reforming of glycerol over Pt catalysts supported on different oxides, Renew. Energy 36 (2011) 595–599.

[16] H.J. Neuburg, J.F. Atherley, L.G. Walker, Girdler-sulphide Process Physical Properties, Atomic Energy of Canada Limited, 1977.

[17] Y. Iwai, T. Yamanishi, S. O'hira, T. Suzuki, M.W. Shu, M. Nishi, H-D-T cryogenic distillation experiments at TPL/JAERI in support of ITER, Fusion Eng. Des. 61–62 (2002) 553–560.

[18] T. Yamanishi, M. Kinoshita, Preliminary experimental study for cryogenic distillation column with small inner diameter, (II), J. Nucl. Sci. Technol. 21 (1984) 853–861.

[19] S. Fukada, H. Fujiwara, Comparison of chromatographic methods for hydrogen isotope separation by Pd beds, J. Chromatogr. A 898 (2000) 125–131.

[20] S. Fukada, Experimental and analytical studies on chromatography of hydrogen–deuterium mixtures with vanadium particle fixed bed, J. Nucl. Sci. Technol. 27 (2012) 642–650.

[21] T. Yamanishi, K. Okuno, Control characteristics of cryogenic distillation column with a feedback stream for fusion reactor, J. Nucl. Sci. Technol. 34 (1997) 375–383.

[22] T. Yamanishi, M. Enoeda, K. Okuno, Experimental study for characteristics of cryogenic distillation column having feedback stream with H-D-T system, J. Nucl. Sci. Technol. 31 (1994) 937–947.

[23] H. Amandusson, L.G. Ekedahl, H. Dunnetun, Hydrogen permeation through surface modified Pd and PdAg membranes, J. Membr. Sci. 193 (2001) 35–47.

[24] A.D. Shugard, G.M. Buffleben, T.A. Johnson, D.B. Robinson, Isotope exchange between gaseous hydrogen and uranium hydride powder, J. Nucl. Mater. 447 (2014) 304–313.

[25] Y.L. Xing, J.J. Cai, L. Li, M. Yang, An exceptional kinetic quantum sieving separation effect of hydrogen isotopes on commercially available carbon molecular sieves, Phys. Chem. Chem. Phys. 16 (2014) 15800–15805.

[26] I. Krkljus, T. Steriotis, G. Charalambopoulou, A. Gotzias, M. Hirscher, H-2/D-2 adsorption and desorption studies on carbon molecular sieves with different pore structures, Carbon 57 (2013) 239–247.

[27] H. Oh, I. Savchenko, A. Mavrandonakis, T. Heine, M. Hirscher, Highly effective hydrogen isotope separation in nanoporous metal-organic frameworks with open metal sites: direct measurement and theoretical analysis, ACS Nano 8 (2014) 761–770.

[28] J. Teufel, H. Oh, M. Hircher, MFU-4 – a metal-organic framework for highly effective H-2/D-2 separation, Adv. Mater. 25 (2013) 635–639.

[29] S.A. FitzGerald, C.J. Pierce, J.L.C. Rowsell, E.D. Bloch, J.A. Mason, Highly selective quantum sieving of D-2 from H-2 by a metal-organic framework as determined by gas manometry and infrared spectroscopy, J. Am. Chem. Soc. 135 (2013) 9458–9464.

[30] T.H. Eyde, D.A. Holmes, Zeolites, in: J.E. Kogel, T.C. Trivedi, J.M. Barker, S.T. Krukowski (Eds.), Industrial Minerals and Rocks: Commodities, Markets and Uses, Society for Mining, Metallurgy and Exploration Inc., United States of America, 2006.

[31] X.Z. Chu, Z.P. Cheng, X.X. Xiang, J.M. Xu, Y.J. Zhao, W.G. Zhang, J.S. Lv, Y.P. Zhou, D.K. Moon, C.H. Lee, Separation dynamics of hydrogen isotope gas in mesoporous and microporous adsorbent beds at 77 K: SBA-15 and zeolites 5A, Y, 10X, Int. J. Hydrogen Energy 39 (2014) 4437–4446.

[32] K. Kotoh, K. Kimura, Y. Nakamura, K. Kudo, Hydrogen isotope separation using molecular sieve of synthetic zeolite 3A, Fusion Sci. Technol. 54 (2008) 419–422.

[33] J. Shang, G. Li, Q. Gu, R. Singh, P. Xiao, J.Z. Liu, P.A. Webley, Temperature controlled invertible selectivity for adsorption of N_2 and CH_4 by molecular trapdoor chabazites, Chem. Commun. 50 (2014) 4544.

[34] J. Shang, G. Li, R. Singh, P. Xiao, D. Danaci, J.Z. Liu, P.A. Webley, Adsorption of CO_2, N_2, and CH_4 in Cs-exchanged chabazite: a combination of van der Waals

density functional theory calculations and experiment study, J. Chem. Phys. 140 (2014) 084705.

[35] J. Shang, G. Li, R. Singh, Q. Gu, K.M. Nairn, T.J. Bastow, N. Medhekar, C.M. Doherty, A.J. Hill, J.Z. Liu, P.A. Webley, Discriminative separation of gases by a ''Molecular Trapdoor'' mechanism in chabazite zeolites, J. Am. Chem. Soc. 134 (2012) 19246–19253.

[36] J. Shang, G. Li, R. Singh, P. Xiao, J.Z. Liu, P.A. Webley, Determination of composition range for ''Molecular Trapdoor'' effect in chabazite zeolite, J. Phys. Chem. C 117 (2013) 12841–12847.

[37] F. Mazzi, E. Galli, The tetrahedral framework of chabazite, Neues Jahrbuch Fur Mineralogie-Monatshefte 10 (1983) 461–480.

[38] D.G. Artiukhin, J. Klos, E.J. Bieske, A.A. Buchachenko, Interaction of the beryllium cation with molecular hydrogen and deuterium, J. Phys. Chem. A 118 (2014) 6711–6720.

[39] A. Czerwiński, Influence of lithium cations on hydrogen and deuterium electrosorption in palladium, Electrochim. Acta 39 (1994) 431–436.

[40] G.T. Kerr, Chemistry of crystalline aluminosilicates. V. Preparation of aluminium-deficient Faujasites, J. Phys. Chem. 72 (1968) 2594–2596.

[41] G.G. Weiss, R.J. Rubin, Random walks: theory and selected applications, in: I. Prigogine, S.A. Rice (Eds.), Advances in Chemical Physics, vol. 52, John Wiley & Sons Inc., Hoboken, NJ, USA, 1982.

[42] M. Nishikawa, T. Shiraishi, K. Murakami, Solubility and separation factor of protium–deuterium binary component system in palladium, J. Nucl. Sci. Technol. 33 (1996) 504–510.

[43] D. Kohen, N. Bamberger, Atomistic simulations of carbon dioxide and nitrogen within zeolites, Presented at the Characterization of Porous Materials: From Angstroms to Millimeters 2015 Conference, 2015.

[44] F. Goltl, J. Hafner, Alkane adsorption in Na-exchanged chabazite: the influence of dispersion forces, J. Chem. Phys. 134 (2011).

[45] M. Calligaris, A. Mezzetti, G. Nardin, L. Randaccio, Cation sites and framework deformations in dehydrated chabazites. Crystal structure of a fully silver-exchanged chabazite, Zeolites 4 (1984) 323–328.

[46] J. Smith, Topochemistry of zeolites and related materials. 1. Topology and geometry, Chem. Rev. 88 (1988) 149–182.

[47] F.N. Ridha, Y. Yang, P.A. Webley, Adsorption characteristics of a fully exchanged potassium chabazite zeolite prepared from decomposition of zeolite Y, Microporous Mesoporous Mater. 117 (2009) 497–507.

[48] D. Kavak, N. Öztürk, Adsorption of boron from aqueous solutions by sepiolite. II. Column studies, Proceedings of the 2nd International Boron Symposium, 2004, pp. 477–485.

[49] V. Inglezakis, S. Poulopoulos, Adsorption, ion exchange and catalysis: design of operations and environmental applications, vol. 3, Elsevier, 2006.

[50] Z. Aksu, F. Gönen, Biosorption of phenol by immobilized activated sludge in a continuous packed bed: prediction of breakthrough curves, Process Biochem. 39 (2004) 599–613.

[51] P. Sivakumar, P.N. Palanisamy, Adsorption studies of basic Red 29 by a non-conventional activated carbon prepared from *Euphorbia antiquorum* L., Int. J. ChemTech Res. 1 (2009) 502–510.